

Magnetic Field Vector Measurement System to Support GPS Navigation

André Diogo Praça Caldeira Martins

andrediogomartins@tecnico.ulisboa.pt

Instituto de Telecomunicações, Laboratório de Instrumentação e Medidas

Instituto Superior Técnico, Lisboa, Portugal

May 2017

Abstract— The magnitude and orientation of terrestrial magnetic field are well known on every spot of the Earth surface. Navigation by GPS has high uncertainty, mostly when the equipment is used in urban areas or by pedestrians.

This work is about the vectorial measurement of terrestrial magnetic field, used in GPS navigation systems to determine heading. To measure the field rigorously it was necessary to dimension, project and build a device that uses a magnetic sensor of three axis, to avoid non-horizontality of measurement surface.

The device was designed using a PC and build with a 3D printer, using Fusing and Deposition of Material method (FDM). It is used an anisotropic magnetoresistance sensor (AMR) and support circuits were designed and printed on circuit boards (PCB), using toner transfer method. To convert the signal from analogic to digital and to communicate with PC it is used a low-cost microcontroller, Arduino UNO.

The calibration algorithm of the sensor was developed in MATLAB, using a fast calibration method for tri-axial magnetometers. The goal of this work is to determine the heading using earth's magnetic field, so it is necessary to collect data points knowing also the position. Two different methods are presented, one that collects points in aleatory positions and other under predetermined positions.

The result of this work is a calibrated system to measure terrestrial magnetic field that provides heading with a known uncertainty.

Keywords— earth magnetic field, magnetometers, AMR, 3D print, FDM, PCB, toner transfer method, fast calibration algorithm, heading

I. INTRODUCTION

GPS navigation systems, mainly pedestrian (PNS) in urban

areas, present high uncertainties. The factors that degrade the GPS signal and consequently affect its accuracy include [1]:

- Delays caused by the ionosphere and troposphere - The satellite signal decelerates as it crosses the atmosphere. GPS calculates an average delay to partially correct this type of error;
- Multipath signal - Occurs when the signal is reflected on objects such as buildings or large rocky surfaces before reaching the receiver. This increases the travel time of the signal, causing errors;
- Receiver clock errors - The receiver clock is not as accurate as the GPS satellite's atomic clock, so there are small differences in time;
- Orbit errors - Also known as ephemeris errors, cause errors in satellite location;
- The number of satellites visible - The more satellites the receiver can reach, the better the accuracy. Buildings, terrain, electronic interference, or dense foliage can block signal reception, causing position errors or signal loss. GPS typically does not work inside buildings, under water and underground;
- Geometry / Layout of satellites - Refers to the relative position of satellites at any time of day. The ideal geometry occurs when satellites are located at wide angles relative to each other. Poor geometry occurs when satellites are aligned or form dense groups.

In addition to the degradation of the signal, there are other factors that cause errors in the GPS positioning calculation. The major source of these errors is the estimation of the direction of motion progression, which is done with the help of sensors and whose readings provide data to calculate the orientation of the magnetic field. Since the intensity and orientation of the Earth's magnetic field are well defined in virtually every place on Earth's surface, accurate measurement of the magnetic field is an important aid in determining the direction of progression. Several animals detect the magnetic field and use it as a form of orientation in their migratory routes. Such evidence has been demonstrated in sea turtles, crustaceans, amphibians and birds [4].

Although the EMF can be represented by a dipole, it does not

serve as an explanation for the origin of the field. The magnetic properties of the materials are not permanent for temperatures above a certain threshold, known as the Curie point, and by studying the behavior of seismic waves it is known that the outer core of the Earth is liquid. Thus, the materials that constitute it (iron and nickel) have temperatures higher than Curie points. Nowadays, the most plausible explanation for the origin of the EMF is known as Dynamo Theory, in which the movement of a good conducting fluid in the outer core (liquid iron) caused by the rotation of the Earth and convection currents generates electric currents and, consequently, a magnetic field. The EMF is a quantity with a vector characterization: it has a direction, an order, a scalar value and a unit of measurement. To unambiguously describe the field three quantities are necessary, for example:

- The intensity of three orthogonal components (X, Y and Z);
- The intensity of the total field and two angles (F, D and I);
- The intensity of two components and an angle (H, Z and D).

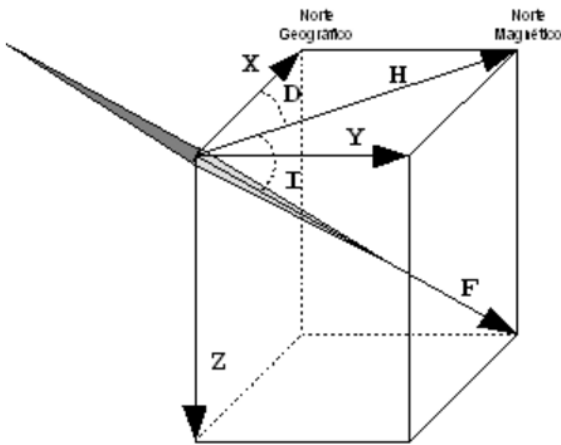


Fig.1 Vector representation of EMF

The intensity of the total field F varies between 24.000nT in South America and 66.000nT between Antarctica and Australia. In mainland Portugal and in the Archipelago of the Azores is currently about 44.000nT, while in the Madeira Archipelago around 40.000nT. Slope I ranges from -90° at the south magnetic pole, indicated by a compass, and 90° at the north magnetic pole. In Continental Portugal and in the Azores this value is around 54° and in Madeira about 45° . The D declination in the Mainland is about $4^\circ W$, while in the archipelagos of Madeira and the Azores around $6^\circ W$ and $12^\circ W$, respectively. The magnetic north is to the geographical North West, so it is negative. The magnetic field, in addition to not being homogeneous, undergoes variations in time, which may be short or long lasting. The first ones are mainly due to solar activity and interaction with the earth's ionosphere and magnetosphere, such as daily variations, magnetic storms (which can give rise to the aurora borealis), magnetic impulses, among others. The slower variations that have their origin in the interior of the external nucleus give the name of secular variation [6].

In contrast to steering techniques using GPS and gyroscope, magnetometers provide measurements that are continuous regardless of external references, and the error does not accumulate over time. However, measurements obtained from low-cost magnetometers, such as those on smartphones, are easily corrupted by several external magnetic disturbances. Thus, a rapid calibration is essential in order to have good estimates [7]. The sources of errors in EMF measurement may be caused by manufacturing errors, deterministic and non-deterministic interferences. While the effects of non-deterministic interferences can be attenuated by filters or even neglected, the others require that the parameters be accurately estimated from the measured data. Deterministic errors can have a different origin. The main sources of errors are caused by ferromagnetic and magnetic materials in the proximity of the sensor, called 'soft iron errors' and 'hard iron errors' [7]. Soft iron errors affect the intensity and direction of the measured field caused by the magnetism generated in the interaction of ferromagnetic materials with an external magnetic field. Hard iron errors result from the memory effect on permanently magnetized materials and are equivalent to a systematic error (bias). There are also errors caused by defects in the manufacture of the sensor, such as non-orthogonality of the axes and different sensitivity values. As such, the magnetometer error refers to the aggregate effects of these errors [7]. According to [8], the magnetometer error effect on the magnetic field can be represented by:

$$h_s = M_s * M_0 * (M_f * h + b_h) + b_s + n$$

where,

h_s is the measured magnetic field value;

M_s is a 3D diagonal matrix of the scale factors that represent the difference in axis sensitivity;

M_0 is a 3x3 matrix that represents the effect of misalignment due to non-orthogonality of the axes;

M_f is a 3x3 matrix that represents the effect of 'soft iron errors';

h is the actual magnetic field value;

b_h is a constant vector representing the effect of 'hard iron errors';

b_s is a constant vector representing the sensor offset;

n is a broadband Gaussian noise.

The equation can be simplified with more general terms:

$$h_s = M * h + b$$

where,

M is a 3x3 matrix that combines scaling factors, non-orthogonality and soft iron errors;

b is the combined systematic error (bias).

The calibration algorithm allows to retrieve h from h_s . The set of intensity points of the real EMF (h) is represented by a sphere of radius equal to the intensity of the EMF. The set of

EMF intensity measurements (h_s) is represented by an ellipsoid.

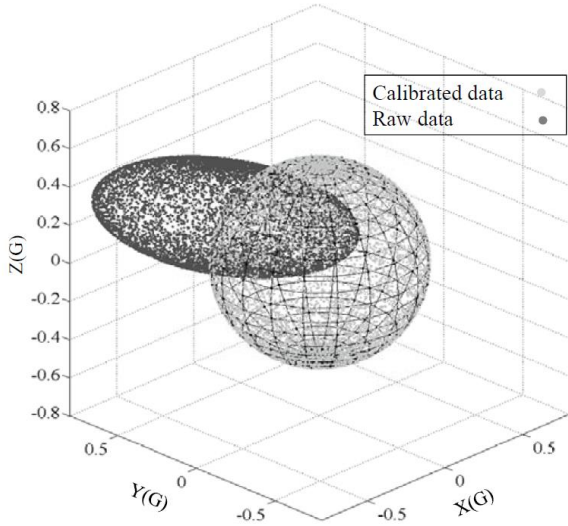


Fig.2 Expected results for h ('Calibrated data') and h_s ('Raw data') [7]

In order to calibrate magnetometers there are several methods described. However, there are aspects that make its applicability difficult, such as the processing capacity and the amount of power available in smartphones [7].

Traditional methods are known by orientation-dependent algorithms, that is, they rely on information from an external reference such as the exact orientation of the EMF. The direction estimates provided by GPS can be used to correct the sensor readings through a Kalman filter, as described in [9]. However, the method is only applicable when the GPS signal is available.

Besides these, there are other techniques that although they are independent of external references, do not consider a complete error model. In these cases the effect of some sources of errors is simplified or ignored, resulting in a lesser complexity of the algorithm and consequent loss of precision. For example, in [10] the effect of ferromagnetic materials is simplified and the effect of possible non-orthogonalities of the axes is neglected. Other methods simplify the process in two dimensions and assume that the sensor will be calibrated by the user, guiding the device to predefined positions so that the algorithm estimates the scalars that transform the resulting ellipsoid into a zero-centered circle as described in [11] and [12]. However, requiring a calibration by the user is not applicable in most everyday situations.

There are methods that still consider a complete error model but are computationally intensive and therefore not suitable for portable devices, such as those described in [13], [14] and [8]. For example, in [8] an ellipsoid fitting algorithm is used, which is based on the fact that the set of measurements form a sphere that, due to the presence of magnetic interference, becomes an ellipsoid. Through the calibration process the magnetic field measurements are processed in order to find the complex scalar

values and the systematic error in order to reverse the transformation.

There are computationally efficient ellipsoid fitting methods based on the least squares method [15]. However, it is necessary to make measurements on a wide spectrum of orientations, in order to obtain the desired precision. Because of the limited sampling capacity of ordinary magnetometers, it takes tens of seconds to collect all points, which is not suitable for real-time applications.

II. BACKGROUND

Magnetometers are instruments in which one or more sensors measure the magnetic flux density B , which can be represented in units tesla or gauss ($1G=10^{-4}T$). Since the magnetic flux density in the air is directly proportional to the strength of the magnetic field, the magnetometer can detect fluctuations in the EMF. Magnetic materials, such as magnetite, create distortions in the magnetic flux lines that are detected by magnetometers. The magnetometer measures the magnetic flux density at the point of the space where the sensor is located, and the intensity decreases in the cubic ratio of the distance to the object. However, the maximum distance to which the object can be detected is directly proportional to the cubic root of the instrument sensitivity [16].

Initially, they were developed and used almost exclusively for navigation and location, especially in the military, aerospace and industrial areas. In recent years, electronic applications, such as smartphones, tablets and laptops, have been developed thanks to advances in MEMS technology as well as in silicone integrated circuits. One of the most recent applications is the e-compass, developed for smartphones, which measures magnetic fields up to 1 nT.

Magnetic sensors can be of two types: analog and digital. The big difference is that the analog sensor circuits can be realized with fundamental electronic components such as resistors, capacitors, coils, diodes, transistors and operational amplifiers. In turn, the digital sensor circuits are a combination of transistors, logic gates and programmable microcontrollers.

If, on the one hand, analogue circuits may present greater difficulties during the implementation phase and are more susceptible to unwanted noise than digital circuits, they also tend to have a lower cost. In this work, the sensor used is an analog sensor, because it fits in the area of Instrumentation and Measurements.

In addition, sensors can be divided into three categories: high sensitivity (lower than nanotesla), low sensitivity (greater than tens of millitesla) and medium sensitivity (interval between both). The sensitivity of a sensor is defined as the variation observed in the output signal caused by the variation of the parameter to be measured, either the factor can be constant in the sensor scale (linear) or it can vary (non-linear).

They can also be separated into two main groups: scalar (measure total magnitude) and vectors (measure magnitude in a given direction). The latter are the sensors of interest, since to accurately measure the earth's magnetic field, three-axis sensors

are required, to avoid errors arising from the non-horizontality of the measurement plane.

There are different types of sensors according to the application area: Hall effect, GMR, MTJ, AMR and Lorentz force. For manufacturers of electronic equipment one of the essential aspects in choosing the magnetic sensor is the cost of production. However, to perform highly accurate measurements, sensitivity is a crucial aspect [17]. The complete information for each model can be found in datasheets (catalogs), made available on the manufacturers' websites.

Sensor	Type	Manufacturer
A1301	Hall	Allegro
A1302	Hall	Allegro
HMC1001/1002	AMR	Honeywell
HMC2003	AMR	Honeywell
HMC1053	AMR	Honeywell
KMZ51	AMR	Philips NXP
AFF755	AMR	Sensittec
AAH002-02	GMR	NVE
AAH004-00	GMR	NVE
AAL002-02	GMR	NVE

Fig. 3 Analog sensors for vector measurement of the magnetic field

There are differences between the characteristics of the sensors according to their effect. To select the most appropriate sensor for the measurement area, it is important to compare the features and highlight their advantages and disadvantages. However, the performance of each sensor can only be fully evaluated during measurements, since the values present in datasheets are only checked under ideal conditions where there are no external influences or manufacturing defects.

	GMR	AMR	HALL
Dimensions	μm	cm	μm
Signal level	High	Medium	Low
Sensitivity	High	Medium	Low
Stability with temperature	High	Medium	Low
Energy consumption	Low	High	Medium
Cost	Low	Medium	Low
Advantages	Dimensions Consumption Sensitivity	Stability of error and sensitivity	Linearity
Disadvantages	Hysteresis Non-linearity Weak SNR	Dimensions Consumption Cost	Signal Sensitivity Stability

Fig. 4 Characteristics of GMR, AMR and Hall sensors [5]

The sensitivity of the MR sensors is much higher than that of the Hall effect sensors, making this group more suitable for EMF precision measurements. In addition, the output signal of the Hall effect sensors is very low and requires high amplification, increasing the unwanted noise effect.

Among the MR sensors, the effect that allows greater sensitivity is the GMR. However, the reduced size of the sensor makes it difficult to do the welding in the laboratory. In addition, GMR sensors have hysteresis, which causes significant errors in measurements, and a weak SNR, for low frequencies. They are also easily corrupted by undesirable strong magnetic fields in the vicinity of the sensor.

AMR sensors are suitable for EMF measurement and have appropriate dimensions for laboratory handling. In addition, the sensitivity and measurement error are well defined and have good stability. Thus, the chosen sensor was Honeywell's HMC1053 [24].

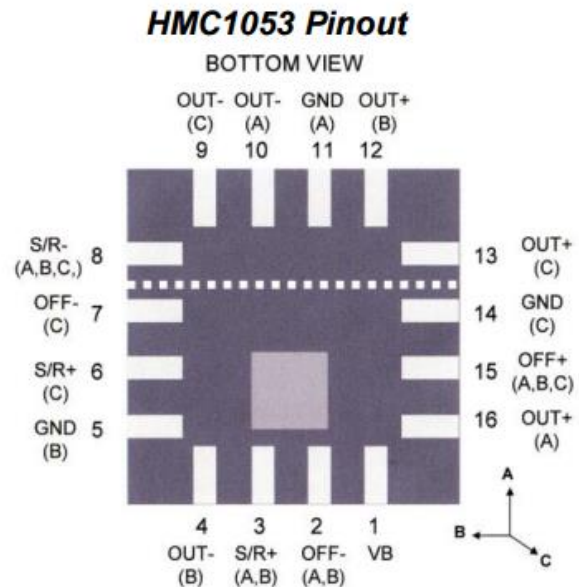


Fig. 4 HMC1053 Pinout [24]

III. IMPLEMENTATION

A. Measuring instrument

To measure EMF using the chosen magnetometer, the following steps were defined:

- Design, size and manufacture of a device to measure EMF in any direction of the Earth's surface
- Design, dimension and manufacture the electronic circuits supporting the sensor, on integrated circuit boards
- Develop an algorithm that calibrates the sensor and provides direction

To measure EMF, it is necessary to use a measuring instrument that meets the following conditions:

- Degrees of freedom allow movement throughout the EMF space;
- The positions allowed by the instrument are programmable and can be set to a good level of accuracy.

The EMF can be represented by a sphere. So, in a system of axes, the degrees of freedom must allow a free movement of 360 degrees in the horizontal plane and 180 degrees in the vertical plane.

To do the 3D drawing of the instrument was used the free distribution software OpenSCAD, for allowing to create models represented by numbers that can easily be adjusted to change the size and shape. The parts have been designed to meet the following conditions:

- Engage a servomotor that rotates freely 180 degrees;
- Couple a stepper that freely rotates 360 degrees;
- Attach a PCB to the sensor;
- Ensure that the fixings are adjustable so that the sensor is positioned in the center of the rotation system

The next step was to print parts created using a 3D printer, model Prusa i3, using Material Fusion and Deposition (FDM) technology.

FDM is an additive manufacturing technology (addition of layered material) commonly used in modeling, prototyping and production applications. A plastic filament is unwound from a coil and routed to an extrusion nozzle, which controls the melting and deposition of the material flow. The nozzle is heated to melt the material and can be moved in both directions, horizontal and vertical (XY), controlled by a computer-aided manufacturing (CAM) software. The piece is fabricated by extruding small beads of thermoplastic material to form successive layers so that each layer of curing material is immediately after extrusion of the nozzle.

The advantage of FDM printing lies in its ability to produce parts and prototypes using thermoplastics such as ABS polymers and PLA biopolymers. These materials become malleable by heating and preserve their shape upon cooling.

In the printing of the pieces of this work PLA was used, a biodegradable polymer made from reusable natural substances, such as corn, potato and sugar cane. It is therefore more environmentally friendly than ABS polymer, formed from petroleum derivatives.

The EAGLE (Easy Applicable Graphical Layout Editor) software was used to draw the PCB. There are diverse types of licenses according to the needs of the project, and for this work was used the free version for university students. There was a need to learn some concepts about its use, using some videos and tutorials.

The program is subdivided into three modules:

- a schematic editor;
- a layout editor;
- an autorouter.

The function of the schematic editor is to create a logical representation of the circuits through the Drag & Drop feature and the electronic component library. The connections are checked by the ERC tool, which detects schematic errors and checks the integrity between schematic and layout. It can create connection classes (NET Class) by defining the width of the tracks and the distance between them.

The layout editor generates the design of the integrated circuits from the schematic. Allows positioning objects at arbitrary

angles and automatically verifies layout rules, such as overlapping of tracks, through the DRC tool.

Autorouter is a tool that uses a multi-threaded algorithm based on cost factors to trace tracks, exploring various solutions and opting for the best one. In more complex cases, the connections that are not resolved by the algorithm must be defined manually.

In the design of PCBs there are factors to consider that made the process difficult, such as:

- The minimum distance between tracks and pads chosen is 0.4mm and the minimum width of the objects is 0.5mm. These values ensure that the result of the layout printing is appropriate to the PCB manufacturing method, but it makes the routing of the tracks more difficult, so it was necessary to use the double face;
- The dimensions and bores of PCBs are in accordance with the location chosen for the fixation in the instrument, which made it difficult to generate the layout and the routing process.

In the manufacture of integrated circuit boards (PCBs) the thermal transfer of toner was used. It is a simple and inexpensive method that can be performed in the laboratory and produces satisfactory results in circuit designs whose copper tracks are not too thin, close or dense, but require some practice, which is obtained by repeating the process experimentally.

The method can be described by the following steps:

1. The layout of the PCB was printed using a laser printer. The print was as dark as possible and a glossy paper was used, so that the ink was partially absorbed. After checking that there were no discontinuities in the lanes, the sheet with the desired dimensions for the PCB was cut;
2. Two types of integrated circuit boards were used, both composed of fiberglass and copper layers. One of the boards was single faced and the other double faced, according to the layout. Each one was cut into the desired dimensions for the PCB and a sandpaper was used to smooth the edges. Thereafter, each plate was washed and cleaned with tap water, neutral detergent and fine steel straw, and paper dried;
3. The printed paper was fixed on the plate using the adhesive tape. A standard iron was used on the paper for about two minutes and at the maximum operating temperature so that the printing ink would stick to the coated side of the plate. With the paper still glued to the plate, it was immersed in a vessel of water and allowed to stand for a few minutes. The thermal shock ensures that the paint is fixed on the copper. Finally, the paper was removed from the plate and corrected for faults that occurred in the lanes using a permanent ink pen.
4. A corrosive solution of powdered iron perchloride was prepared by mixing it with water. The mixture generates a lot of heat and the procedure requires exceptional care, such as the use of protective equipment and that the place is prepared to make the extraction of gases. The perchlorate was placed in the water in a ratio of 500 grams to 1 liter of water, slowly dissolving it. No stirring instruments or metal containers were used, only glass or plastic. The plate was completely covered by the mixture and slightly sloped, with the copper side facing up. The corrosion time lasted from 10 to 30 minutes, depending

on the size of the plate and the ambient temperature. One technique used to reduce the corrosion time was to constantly stir the vessel and move the plate using plastic forceps. After noting that the plate was completely corroded and did not show traces of copper, it was carefully removed from the vessel and washed with water.

5. With an alcohol-soaked cloth, the ink was completely removed from the print until the copper tracks were uncovered. The cleaning was completed using a steel wool.

6. Finally it was necessary to use a drill to do the mounting holes and to interconnect the existing tracks on both sides.

After performing the method described for the three PCB boards of the instrument, it was necessary to solder the electronic components to the designated locations during the layout design. Welding requires some practice and can be performed in the laboratory provided that the components meet a minimum distance between them and are not too small. This was a concern during the design phase, due to the importance it has both in the manufacturing phase and in the welding phase. In the case of the PCB containing the magnetometer, the greatest difficulty was due to the reduced size of the sensor legs. To conclude, the PCB's copper tracks were protected from oxidation by spraying the plate with an acrylic spray coating. However, this procedure was only carried out after the operation of the PCB was tested, since the coating makes the desoldering process very difficult.

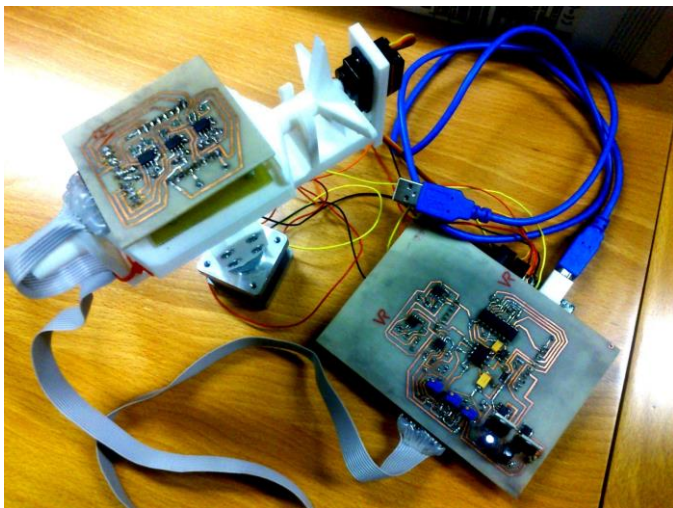


Fig.5 Measuring instrument

B. Microcontroller

The HMC1053 magnetometer is an analog sensor that provides a continuous response signal proportional to the magnitude to be measured. Before being sent to a computer it must be converted into its digital form. In addition, it is necessary to power the sensor and control the motors: servomotor and stepper. These functionalities can be realized using a low-cost microcontroller, the Arduino UNO.

The Arduino UNO is based on the 8-bit ATmega328 microcontroller. It has 14 digital input/output pins (6 can be used as PWM outputs), 6 analog inputs, a USB port and a Reset button. To connect it, simply plug to a computer through the USB port or power through an AC-DC adapter. It allows to feed other devices through the 5V and 3.3V outputs, but for this work only the 5V output was used.

To create the Arduino communication interface with the measuring instrument, the PCB board was designed with the same configuration and pinout dimensions as the Arduino so it can be coupled, thus avoiding additional wires.

The 5V pin of the Arduino is responsible for powering the circuits of the measuring system, the GND pin supplies the ground and the inputs A0, A1 and A2 receive the analog signal. The digital outputs are responsible for operating the motors.

The instructions are sent to the microcontroller via a computer application, Arduino IDE (Integrated Development Environment), which includes a code editor capable of compiling and loading programs in C language, a serial monitor to view received data or send data in time Scripts to perform the most common functions.

To control the engines there are libraries that make the process simple and intuitive. On the website (<https://www.arduino.cc/>) you can find examples for the most common functions, including motor control and sensor data collection. Set/Reset functionality was operated by 'digitalWrite ()' instruction, sending 'LOW' pulses to Reset and 'HIGH' to Set, 100 milliseconds later, according to sensor datasheet.

C. Calibration Algorithm

In [7] a new iterative calibration algorithm for three-axis magnetometers is proposed, which performs the estimation and compensation of the effects of the deterministic interference parameters, making use of only nine different measures collected during the rotation of the sensor. In addition, it has a low computational cost to meet the limitations of mobile devices, and does not use predefined positions during calibration, exploring the user's natural movement. The results of the simulations and empirical evaluations made by the author confirm that the proposed method is better than conventional models, both in terms of precision and reliability and in terms of unwanted noise. The algorithm has fast convergence, suitable for real-time applications, and the efficiency is independent of the initial interference parameters. Like the existing methods, the performance of the algorithm degrades with the non-deterministic noise level.

The purpose of the calibration is to estimate the values of M and b to calculate h from the measured values h_s . The method used is iterative, so the parameters are estimated in the form \hat{M}_k e \hat{b}_k , where k is the order of iteration, and are expected to converge to their real value.

$$\mathbf{h}_s = \left(\prod_{i=0}^k \tilde{\mathbf{M}}_i \right) * \hat{\mathbf{h}}_k + \sum_{i=0}^k \tilde{\mathbf{b}}_i$$

$$\left(\prod_{i=0}^k \tilde{\mathbf{M}}_i \right) = \hat{\mathbf{M}}_k, \quad \sum_{i=0}^k \tilde{\mathbf{b}}_i = \hat{\mathbf{b}}_k$$

The initial values $\tilde{\mathbf{M}}_0$ and $\tilde{\mathbf{b}}_0$ can be defined arbitrarily, through a matrix (for example, identity matrix) and a vector.

$$\hat{\mathbf{h}}_k = (\hat{\mathbf{M}}_k)^{-1} * (\mathbf{h}_s - \hat{\mathbf{b}}_k)$$

Considering that the intensity of the real magnetic field is constant and known, a factor for the error is defined as the difference between the field intensity result at each iteration and its real value.

The last term of the final expression for the error is practically null at the end of the iterations, since the factor $\tilde{\mathbf{b}}_k$ converges to zero. Still, there are nine parameters to calculate, six of which belong to Q_k and three to $\tilde{\mathbf{b}}_k$. Because the algorithm is based on the magnetic field strength, three degrees of freedom are lost in the calculation of Q_k . However, the existing state of the art on the problem has shown that this does not significantly deteriorate the results.

The algorithm converges when the values of $\tilde{\mathbf{b}}_k$ are close to zero and $\tilde{\mathbf{M}}_k$ is the identity matrix.

The software used to write the algorithm was MATLAB, a tool based on C-language, appropriated for operations between matrices and representation of the results graphically. In this case, there was already solid knowledge about the use of the program, because it is widely used in projects and laboratory classes during the course.

The algorithm was written based on the flowchart presented and on the equations described in [7]. The result is a matrix \mathbf{M} (3x3) and a vector \mathbf{b} (3x1) that is used in the calculation of h from the measurements made by the sensor.

In addition to the calibration algorithm, a MATLAB routine was developed to establish communication with the Arduino. First of all both platforms must know the Baud Rate and the serial port that they will use to communicate. Then, using commands, platforms send data (Write) and receive data (Read) from a buffer.

Arduino loads a program that, when requested by a serial command, collects the data of the sensor and writes in the buffer, ready to be read by MATLAB.

MATLAB runs a script that sends strings with measurement requests to Arduino and reads data from the buffer.

IV. RESULTS

To perform the calibration of the sensor, two different methods were used to collect points:

- Method 1 - gather the points according to random positions;
- Method 2 - collect points according to predefined positions.

A. Method 1

In an outdoor environment, free of magnetic disturbances inside buildings, measurements were collected so that the axes described rotations from all angles. The measurements are described by x, y and z coordinates, which correspond to the variation of the voltage at the sensor output with the magnetic field incident on the axes. A constant number of measurements was defined for each variation of the zenith angle.

Using MATLAB, the measurements were stored in a matrix and represented.

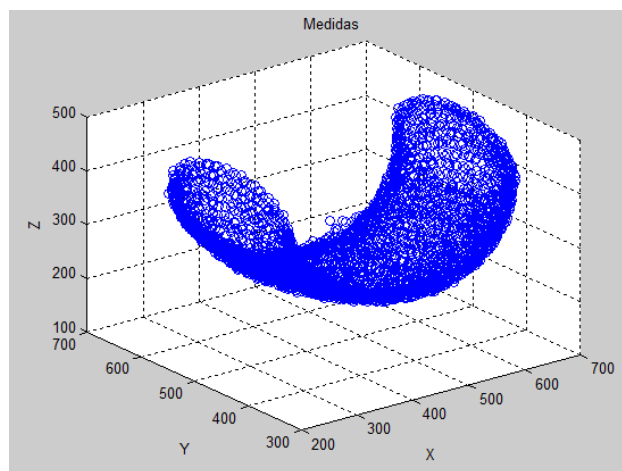


Fig. 6 Sensor Measurements

Figure 6 represents the total space of measurements of the magnetic field. Each circle of points is on a different axis system, and it is necessary to place them on the same reference frame. To do this, it was necessary to calculate the mean value of the measurements for each axis and subtract it from each measure of the corresponding axis. Because the measures do not follow a uniform distribution, the average is the sum of all measures divided by the number of measures. Then, the same calculation was performed for each variation of the zenith angle, which means that there are several mean values corresponding to the number of measured zenith angles.

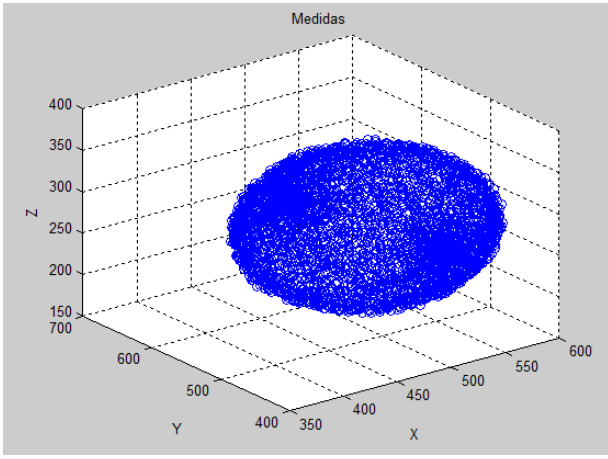


Fig. 7 Measurements of the sensor in the same reference

Figure 7 shows the space of measurements collected by the sensor, referenced to the same axis system. The 'cloud' of ellipsoid points corresponds to the predicted result for the magnetic field by the calibration algorithm. However, for the algorithm to work well it is necessary that the deviations in the measurements be eliminated and corrected to respect the equations of an ellipsoid using the ellipsoid fitting method. For this, the `ellipsoid_fit` function [27] was used to obtain the ellipsoid surface, and the MATLAB function 'ellipsoid', to generate the surface points. The ellipsoid points were generated for a matrix of 60 azimuthal positions, representing a sensitivity of 6 degrees ($360^\circ / 60 = 6^\circ$) and an average error of 3 degrees ($6^\circ / 2 = 3$) and maximum of 6 degrees, in case of measurement being the same distance between two positions.

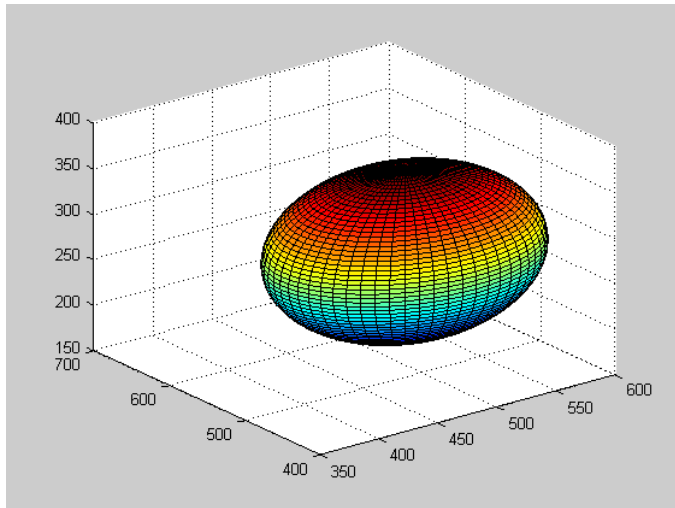


Fig. 8: Ellipsoid surface

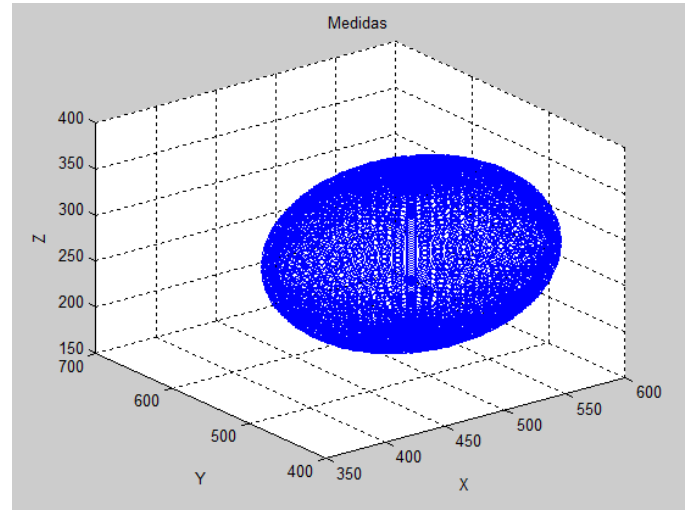


Fig. 9 Set of ellipsoid points

Figures 8 and 9 represent the generated surface and the points corresponding to that surface.

Now that the 'cloud' of points can be well described through the ellipsoid equations, the next step is the application of the fast-calibration algorithm described in Chapter 5. Calibration Algorithm. For this, nine points of the ellipsoid are used in random directions, from which the matrix M and the vector b of the equation are generated:

$$h_s = M * h + b$$

at where,

M is a 3x3 matrix that combines scaling factors, non-orthogonality and soft iron errors;
 b is the combined systematic error (bias);
 h_s is the measured magnetic field value;
 h is the actual magnetic field value.

The calibration algorithm allows to retrieve h from h_s , through the equation:

$$h = M^{-1} * (h_s - b)$$

The operation is performed for all points of the ellipsoid.

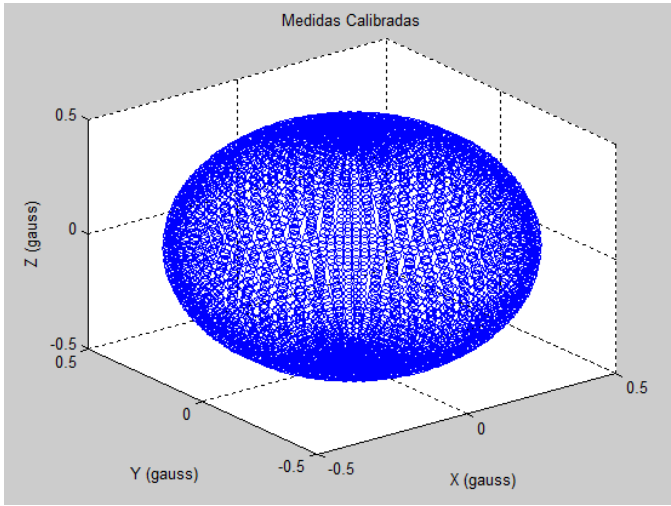


Fig. 10 Calibrated Measures

The figure 10 represents the measurements of the magnetic field calibrated according to a sphere of center at the origin and radius equal to the intensity of the magnetic field, approximately 0.5 gauss. The result is in accordance with the predicted by the calibration algorithm and with the theoretical values of the terrestrial magnetic field.

Each measurement is associated with its position in the sphere, as a function of the azimuth angle φ and the zenith angle θ , calculated according to the equations:

$$\theta = \cos^{-1} \frac{Z}{r}$$

$$\varphi = \tan^{-1} \frac{X}{Y}, \quad [-\pi, \pi]$$

The calibration process is now complete.

B. Method 2

The alternative method of calibration assumes that the measurements are collected according to a direct trihedron, considering two angles that give any spatial orientation.

The azimuth angle φ varies between $[-180, +180]$ degrees, where $\varphi = 0$ corresponds to point in the geographic north direction. The zenith angle θ varies between $[-90, +90]$ degrees, Where $\theta = -90$ corresponds to point downwards in the vertical of the place and $\theta = +90$ corresponds to pointing upwards. Thus, $\varphi = 0$ and $\theta = 0$ corresponds to point in the geographic north direction according to the horizontal plane.

To perform a complete rotation in the horizontal plane it is necessary to impose $\theta = 0$ and to change φ between $[-180, +180]$. To obtain 50 points in the horizontal plane it is necessary that φ take values in the interval $[-180: 7.2: +179]$. For other values of θ there will be less than 50 points, since the upper and lower constant latitude circles are smaller. To maintain a

uniform density, it is necessary to obtain several points k , according to $k(\theta) = 50 * \cos \theta$, approximately.

In this way, the positions of the measurements are already known at the outset, simply obtaining the magnetic field strength for each position. This corresponds to calculating the modulus of the vector represented by the three coordinates, according to:

$$r = \sqrt{X^2 + Y^2 + Z^2}$$

The vector module is the distance from the point representing the measurement to the center of the sphere, that is, it corresponds to the radius of the sphere.

Using a MATLAB, a sphere of points was generated according to the positions already described and a value r was calculated for each measurement performed according to the positions of the sphere.

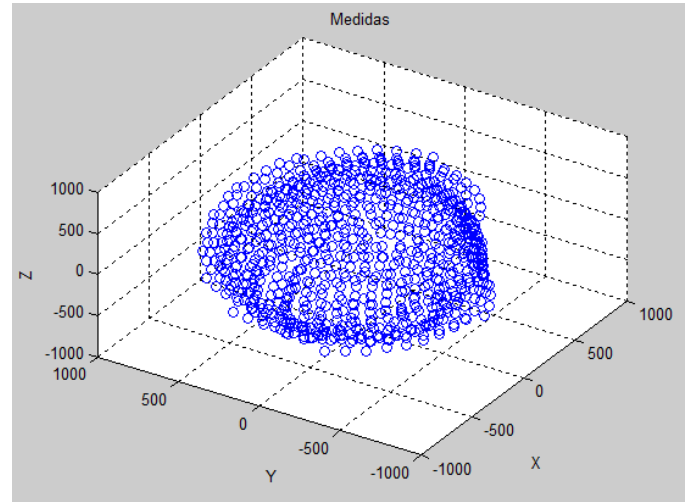


Fig. 11 Sensor Measurements

The figure represents the result of the combination of the positions defined by the sphere and the radius obtained from the measurements. The result is a 'cloud' of points in the form of an ellipsoid.

From this step, the procedure is the same as that followed for Method 1.

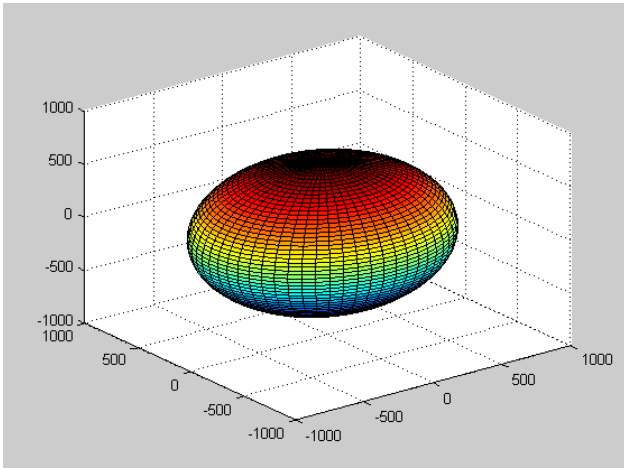


Fig. 12 Ellipsoid surface

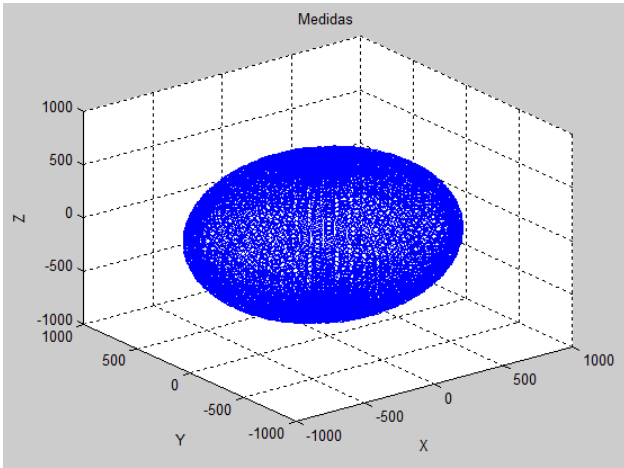


Fig. 13 Set of ellipsoid points

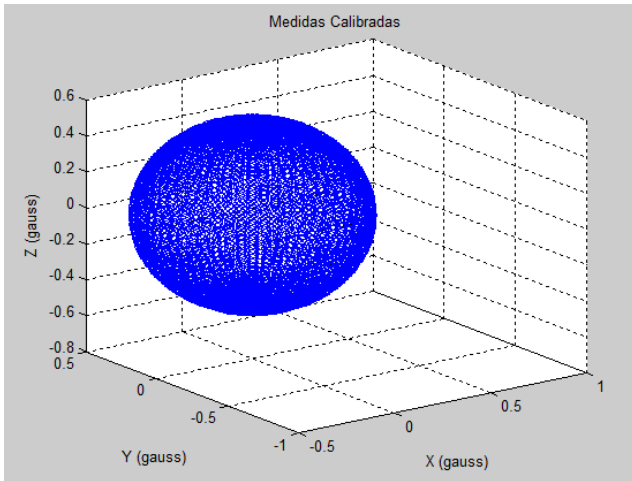


Fig. 14 Calibrated Measures

Figures 12, 13 and 14 represent the results obtained in the calibration. The result is a center sphere at the origin and radius equal to the intensity of the magnetic field, approximately 0.5 gauss. The result is in accordance with the predicted by the

calibration algorithm and with the theoretical values of the EMF.

Each measurement is associated with its position in the sphere, as a function of the previously known azimuth angle φ and the zenith angle θ . The calibration is now complete.

C. Determination of heading

To obtain the heading of the user, for any spatial orientation, using only the magnetic field measurements provided by the magnetometer, calibration method 2 was used since the measurements are already positioned according to a single reference. Method 1, because it requires that the measures be repositioned in relation to the same reference, allows to obtain directions only for a predefined plane. For directions to be obtained for any spatial orientation, the calibration method requires zenith angle data, which can be obtained through an accelerometer or a gyroscope.

To obtain the direction of the user, a measurement h_s was made with the measuring instrument oriented in the same direction as the user. Then, the measure was applied in the equation:

$$h = M^{-1} * (h_s - b)$$

The same parameters M and b obtained during the calibration of method 2 were used. Then the Euclidean distance of the calibrated measurement (X', Y', Z') was calculated at all points of the calibration sphere (X, Y, Z) according to the equation:

$$d = \sqrt{(X - X')^2 + (Y - Y')^2 + (Z - Z')^2}$$

The point (X, Y, Z) that minimizes the distance d is the point representing the measurement made on the calibration sphere.

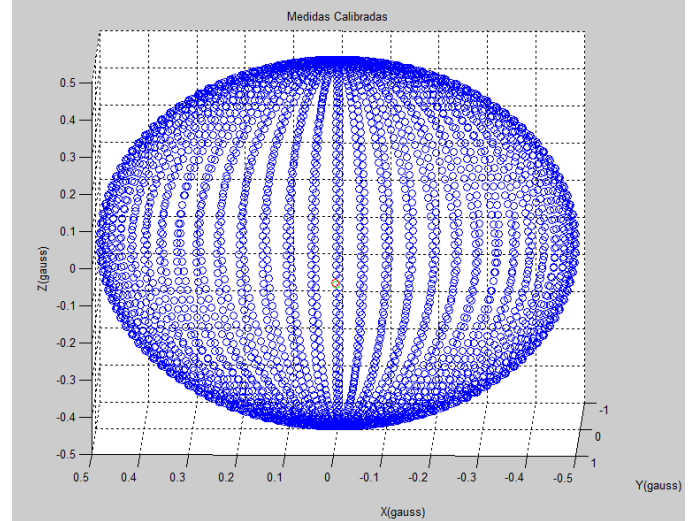


Fig. 15 Determination of user heading

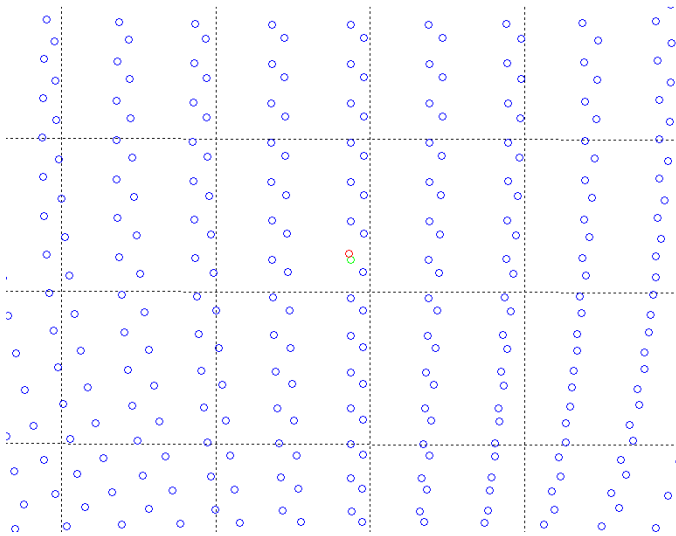


Fig. 16 User position (red) and calibration ball point (green)

In Figures 16 and 17 the point corresponding to the user's position is shown in red and the calibration ball point minimizing the distance is marked in green. It is possible to determine that the user is directed to 0° North, which was confirmed by a compass. Precision at the azimuth angle is affected by the magnetic declination, which is not considered.

V. CONCLUSIONS

The results of this work demonstrated that it is possible to obtain heading of movement only based on EMF vector measurement, with a known uncertainty, taking advantage of the built measuring instrument. However, the cost of this method is the need to calibrate the sensor according to predefined positions that represent all spatial directions, which requires a measuring instrument with some precision, in addition to being a time-consuming process.

A method is introduced that eliminates the need to orient the sensor under predefined positions and takes advantage of the fast calibration algorithm used, reducing the calibration time to just a few seconds. However, the cost of this improvement is that the heading can only be determined for a single zenith angle. To obtain the direction in any spatial orientation it is necessary to resort to data from other sensors that provide additional information. In future works, it is possible to use another sensor, such as an accelerometer or a gyroscope, and integrate the data into the calibration.

The AMR magnetometer proved to be a good option to measure EMF because of the high sensitivity at low frequencies. Despite the external magnetic disturbances and the noise generated by the sensor support circuits, the measurements corresponded to what was expected.

It is possible to eliminate the need to connect the measuring instrument to a USB port, using batteries to power the sensor and circuits, and using Bluetooth communication between the notebook and the instrument. Thus, the instrument may be outside the range of an important source of magnetic

disturbance, such as the laptop, and the user has more freedom to perform measurements, especially in height, where magnetic disturbances are reduced.

ACKNOWLEDGMENTS

My first words of acknowledgment are dedicated to my parents, Adelaide Martins and Fernando Martins, who gave me all the support so I could fulfill this important goal in my life, and to my girlfriend, Regina de Souza, for the support and motivation. I thank Prof. Artur Ribeiro and Prof. Francisco Alegria for their availability and for helping me to develop my knowledge in instrumentation and algorithms.

I thank the colleagues I met at the Instrumentation and Measurement Laboratory, especially Tiago Rocha and Dário Pasadas, who helped me to build the measurement instrument. Finally, I thank the colleagues with whom I studied during my academic journey.

REFERENCES

- [1] "What is GPS?", Garmin Ltd., 2014 (<http://www8.garmin.com>)
- [2] M. Schmandt, "GIS Commons: An Introductory Textbook on Geographic Information Systems; Chapter 2: Data Input", 2009 (<http://giscommons.org>)
- [3] J. Fischer, "Navigating with more than just GPS; Wanted: More Satellites", maio de 2012 (<http://electronicdesign.com>)
- [4] K. J. Lohmann et al, "Magnetic maps in animals: nature's GPS", julho de 2007 (<http://jeb.biologists.org>)
- [5] K. Mohamadabadi, "Anisotropic Magnetoresistance Magnetometer for Inertial Navigation Systems", Electronics, Ecole Polytechnique X, 2013 (<https://tel.archives-ouvertes.fr/tel-00946970>)
- [6] Página Oficial do IPMA (<http://www.ipma.pt/pt/enciclopedia/geofisica/geomagnetismo>)
- [7] S. Hoseinitabatabaei et al., "A Fast Calibration Method for Triaxial-Magnetometers", IEEE Transactions on Instrumentation and Measurement, vol. 62, n. 11, pp. 2929 - 2937, agosto de 2013
- [8] V. Renaudin, M.H. Afzal, and G. Lachapelle, "Complete Triaxis Magnetometer Calibration in the Magnetic Domain," Journal of Sensors, vol. 2010, pp. 1-10, 2010.
- [9] R. Jirawimut, P. Ptasiński, V. Garaj, F. Cecelja, and W. Balachandran, "A method for dead reckoning parameter correction in pedestrian navigation system," IEEE Transactions on Instrumentation and Measurement, vol. 52, no. 1, pp. 209-215, 2003
- [10] F. Camps, S. Harasse, and A. Monin, "Numerical calibration for 3-axis accelerometers and magnetometers," in IEEE International Conference on Electro/Information Technology, 2009. eit '09., Windsor, ON, 2009, pp. 217-221
- [11] L. Fang et al., "Design of a wireless assisted pedestrian dead reckoning system- the NaveMote experience," IEEE Transactions on instrumentation and measurements, vol. 54, no. 6, pp. 2342-2358, 2005

LIST OF ACRONYMS

[12] C. Huang, Z. Liao, and L. Zhao, "Synergism of INS and PDR in Self-Contained Pedestrian Tracking With a Miniature Sensor Module," *IEEE Sensor journal*, vol. 10, no. 8, pp. 1349 - 1359, agosto de 2010

[13] C.C. Foster and G.H. Elkaim, "Extension of a two-step calibration methodology to include nonorthogonal sensor axes," *IEEE Transactions on Aerospace and Electronic Systems*, vol. 70, no. 3, pp. 1070-1078, julho de 2008

[14] E. Dorveaux, D. Vissiere, A.-P. Martin, and N. Petit, "Iterative calibration method for inertial and magnetic sensors," in *Proceedings of the 48th IEEE Conference on Decision and Control, 2009 held jointly with the 2009 28th Chinese Control Conference. CDC/CCC 2009, Shanghai, 2009*, pp. 8296-8303

[15] J. Fang, H. Sun, J. Cao, X. Zhang, and Y. Tao, "A Novel Calibration Method of Magnetic Compass Based on Ellipsoid Fitting," *IEEE Transactions on Instrumentation and Measurement*, vol. 60, no. 6, pp. 2053-2061, junho de 2011

[16] P.Jain, "Magnetometers", *Engineers Garage*, 2012 (<http://engineersgarage.com>)

[17] Y.Cai et al., "Magnetometer basics for mobile phone applications", *Memsic*, fevereiro de 2012 (<http://memsic.com>)

[18] H.Mason, "Basic Introduction to the use of Magnetoresistive Sensors", *Zetex Application Note 37*, setembro de 2003 (<http://diodes.com>)

[19] A1301/A1302 Datasheet, *Allegro MicroSystems*, 2013 (<http://allegromicro.com>)

[20] Basic Knowledge of AMR Sensors (Magnetic Switches), *Murata*, (<http://murata.com>)

[21] HMC1001/HMC1002/HMC2003 Datasheet, *Honeywell* (<http://honeywell.com>)

[22] HMC1051/HMC1052L/HMC1053 Datasheet, *Honeywell*

[23] KMZ51 Datasheet, *NXP Semiconductors*, 1998 (<http://nxp.com>)

[24] AFF755 Datasheet, *Sensitec*, 2011 (<http://sensitec.com>)

[25] NVE AAH002-02/AAH004-00/AAL002-02 Datasheet, *NVE Corporation*, (<http://nve.com>)

[26] T. Ozyagcilar, "Calibrating an eCompass in the Presence of Hard and Soft-Iron Interference," *Freescale Semiconductor, Application Note 2012*.

[27] Yury, "Ellipsoid fit", *MathWorks*, 2015 (<https://www.mathworks.com/matlabcentral/fileexchange/24693-ellipsoid-fit>)

ABS – Acrylonitrile-Butadiene Styrene

AMR – Anisotropic Magnetoresistance

CAD – Computer-Aided Design

EAGLE – Easy Applicable Graphical Layout Editor

EMF – Earth Magnetic Field

FDM – Fused deposition modeling

GMR – Giant Magnetoresistance

GPS – Global Positioning System

INS – Inertial Navigation System

MATLAB – MATrix LABoratory

MEMS – Micro-Electro-Mechanical Systems

MINAV – Magneto Inertial Navigation System

MTJ – Magnetic Tunnel Junction

MR – Magnetoresistance

PCB – Printed Circuit Board

PLA – PolyLactic Acid

PNS – Pedestrian Navigation System